



Quad band metal-dielectric-metal perfect absorber to selective sensing application

Seyed Amin Khatami¹ · Pejman Rezaei¹ · Pouria Zamzam¹

Received: 24 September 2021 / Accepted: 22 June 2022 / Published online: 24 August 2022
© The Author(s), under exclusive licence to Springer Science+Business Media, LLC, part of Springer Nature 2022

Abstract

In this article, we have managed to achieve a quad-band perfect classical absorber in the terahertz band. In this proposed structure, which consists of three layers that the top and bottom layers made of gold and a dielectric layer, is located in middle layer. The results show that this structure has four perfect absorption bands with an average absorption of 98.22% at frequencies of 1.36, 2.6, 3.68, and 4.36 THz. To better understand the absorption mechanism, an equivalent circuit related to the proposed structure is presented. We have also shown that the percentage of absorption of the proposed absorber has increased due to the loss of the middle layer. Finally, the distribution of the electric fields is shown at each of the absorption frequencies. Due to its four bands, this absorber has potential in imaging, selective sensing, and photodetector applications.

Keywords Terahertz · Absorber · Perfect absorption · Quad-band · Multi-band · Metamaterial

1 Introduction

In recent years, in the mm-wave frequencies, many activities have been done in various fields such as antennas, filters, sensors, etc. (Khatami et al. 2020; Mousavi et al. 2017, 2019; Kiani et al. 2020, 2021a, b; Sharbati et al. 2016; Ikram et al. 2020; Khani et al. 2018). Microwave absorbers are among these areas, which have recently been studied in various designs and shapes, and examples of them are given in Yu et al. (2019), Lim and Sungjoon (2019), Ghosh and Kumar (2017) and Kundu et al. (2016).

Today, the focus of many researchers in communication has shifted to terahertz frequencies. Examples of devices that operate in this frequency range are introduced in Khani et al. (2019, 2020a, b, 2021). One of the structures that are significantly used in optical devices is metamaterial structures. Metamaterials are engineered materials which are not found in nature. It is a unique property that causes it to exhibit various characteristics such as negative refraction, cloaking, negative permittivity, perfect absorption, and so on. So, the metamaterial-based absorber was firstly investigated in

✉ Pejman Rezaei
prezaei@semnan.ac.ir

¹ Electrical and Computer Engineering Faculty, Semnan University, Semnan, Iran

2008 (Askari and Hosseini 2020a, 2020b; Askari 2021; Landy et al. 2008). The primary function of the terahertz absorber is absorbing terahertz waves. This process is based on two hypotheses: one wave of collision with the structure is lost inside the structure, and the other is the wave becomes to surface waves. In general, it should satisfy the following formula:

$$A = 1 - R - T \quad (1)$$

Given that we are looking for 100% absorption, according to the above formula, T and R should be as close as zero.

Graphene is composed of single-layer carbon atoms, a two-dimensional honeycomb structure. Since it discovered in 2004 by Novoselov, it has been highly regarded by researchers for its good electrical, optical, and mechanical properties. Today, graphene has many applications in electrical, photonic, and sensor devices, and so on Meng et al. (2017), Jafari Chashmi et al. (2020a, 2020b), Ghods and Rezaei (2018a), Esfandiari et al. (2021) and Danaeifar and Granpayeh (2020). Besides, the surface conductivity of graphene can be changed by Fermi energy, and different Fermi levels can be obtained by biased voltages or chemical doping.

This feature can be used to tunable optical devices such as antennas, filters, absorbers, etc. Examples of graphene-based optical devices are given in Bian et al. (2021), Kiani et al. (2021c), Kazemi (2021), Norouzi-Razani and Rezaei (2022), Alizadeh et al. (2022), Soheilifar (2018a) and Jiang and Chen (2022). A four-leaf clover-shaped reconfigurable patch antenna based on graphene is presented in Shimatani et al. (2022). In Upender and Kumar (2022), a high Q-factor compact, and reconfigurable THz aperture antenna based on graphene loads for detecting breast cancer cells are introduced.

A compact reconfigurable V-shaped dipole antenna in THz frequency is presented in Jafari Chashmi et al. (2019). In Zamzam et al. (2021), a quad-band, polarization-insensitive metamaterial perfect absorber based on bi-layer graphene in the terahertz regime is introduced. A dual-band terahertz absorber based on graphene periodic arrays of disks and ribbons: circuit model approach is given in Aghaee and Orougi (2021). In Mishra and Panwar (2020), investigation of graphene fractal frequency selective surface loaded terahertz absorber is introduced. In Soheilifar (2018b) wideband optical absorber based on plasmonic metamaterial cross structure is designed and simulated.

In Ebrahimi (2020), optical absorber based on the self-similar cylindrical element for detecting optical material is designed. Also, in Zamzam and Rezaei (2021), a terahertz dual-band metamaterial perfect absorber based on metal-dielectric-metal multi-layer columns is introduced.

Furthermore, many absorbers are used in the GHz frequency band. In Ghods and Rezaei (2018b) ultra-wideband microwave absorber based on uncharged graphene layers is introduced. A stretchable metamaterial absorber with a deformation compensation design at microwave frequencies and an adaptive broadband radar absorber based on tunable graphene are presented in Zhou et al. (2018) and Aloia et al. (2016), respectively. Also, classical absorbers are provided in Yi et al. (2019) and Hu et al. (2016).

Multi-band absorbers in the terahertz band have also been considered by researchers today, examples of those can be seen in Chen and Fan (2015), Wang and Wang (2015), Meng et al. (2018) and Arezoomand et al. (2015).

In the proposed structure, we have achieved a quad-band absorber with the same 3-layer or classical terahertz absorber. This structure is sensitive to incident wave polarization and insensitive to the angle of the direction of the incident wave. This

structure has four absorption bands with absorption peaks of 96.46%, 99.82%, 97.74%, and 98.86% at frequencies of 1.36, 2.6, 3.68, and 4.36 THz. Compared to the multi-band absorbers introduced in previous works, the proposed absorber, which consists of a metal strip, has the advantage that it is one of the simplest structures for perfect multi-band absorbers. Therefore, using these types of structures can overcome the complexities of fabrication and the large size of the unit cell associated with absorbers. Accordingly, such a simple device can prepare an optimal absorption manner and operation for selecting the terahertz frequency band and more practical applications. We believe that the proposed absorber has the potential for filtering, detection, and imaging.

2 Method and theory

The proposed absorber structure is shown in Fig. 1. Figure 1a shows the side view and Fig. 1b shows the top view of the proposed structure.

This structure consists of three layers of metal-dielectric-metal, which the material of the upper and lower layers of the proposed absorber is gold with a conductivity of 4.56×10^7 S/m (Kiani et al. 2021c). The thickness of gold in the upper and bottom layers are $t_1 = 0.2 \mu\text{m}$ and $t_2 = 0.5 \mu\text{m}$ (respectively). The substrate (middle layer) is the SiO_2 with a dielectric constant of 3.24 and loss tangent of 0.066 and a thickness of $h = 11.5 \mu\text{m}$ (Hu et al. 2016). The curve of the real and imaginary part of the dielectric constant with the loss tangent of SiO_2 is shown in Fig. 2.

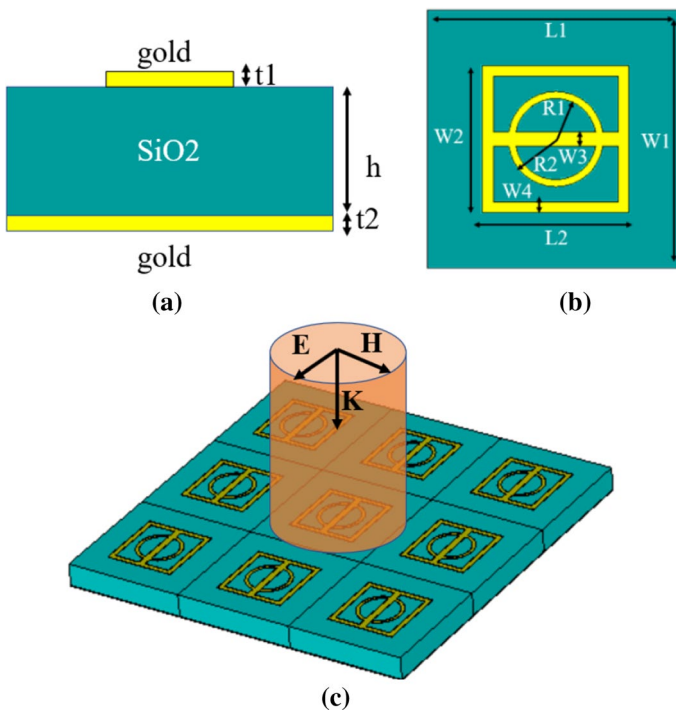
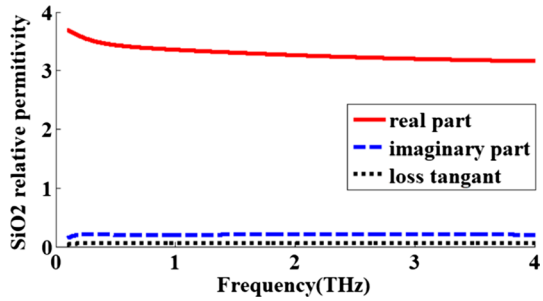


Fig. 1 Proposed absorber configuration **a** side view **b** top view **c** perspective view

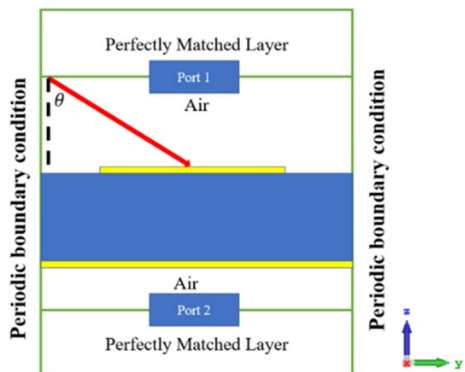
Fig. 2 Specifications of SiO₂ material



The designed dimensions of the structure are $W1=70$, $L1=70$, $W2=40$, $L2=40$, $W3=4$, $W4=3$, $R2=13$, and $R1=11$ μm . The boundary conditions applied to analyze the proposed absorber are illustrated in Fig. 3. As it has been shown in this figure, in the X and Y direction, the boundary conditions were periodic and in the Z direction, the perfectly matched layer boundary conditions are utilized. In this proposed absorber, the plane wave is used as the excitation source, and it should be noted that the incident electromagnetic wave propagates vertically along the negative z-axis. Full-wave simulation of this structure has been done using CST software and in the frequency domain. Also, the finite element method (FEM) has been used to analyze this structure. All the meshing parameters related to the proposed adsorber are given below: mesh type=tetrahedrons, mesh number=18,005, min. edge length=0.100147, max. edge length=26.249, Min. quality=0.0016, max. quality=0.99.

Given the classical proposed structure, its equivalent circuit is shown in Fig. 4. As shown in Fig. 4a, this circuit is equivalent to 3 parts A to D, each of them has its own job description. The bottom layer returns all the incident wave power due to its greater thickness than the penetration depth of the terahertz wave. Therefore, the bottom layer in part A of the circuit is a short circuit. Part B of the equivalent circuit, denoted by Y_d , is called the ambient admittance of the middle layer, which is strongly dependent on the height of this lossy layer. Part C corresponds to the top layer of the structure; this part consists of series RLCs that are connected in parallel with a capacitor. Each of these series RLCs is related to one of the resonance frequencies, and the intermediate capacitor between these RLCs is in fact isolating these output frequencies due to one of

Fig. 3 General schematic of boundary conditions used to analyze the proposed absorber



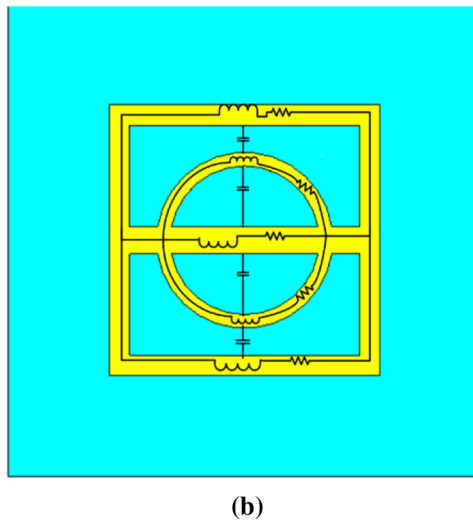
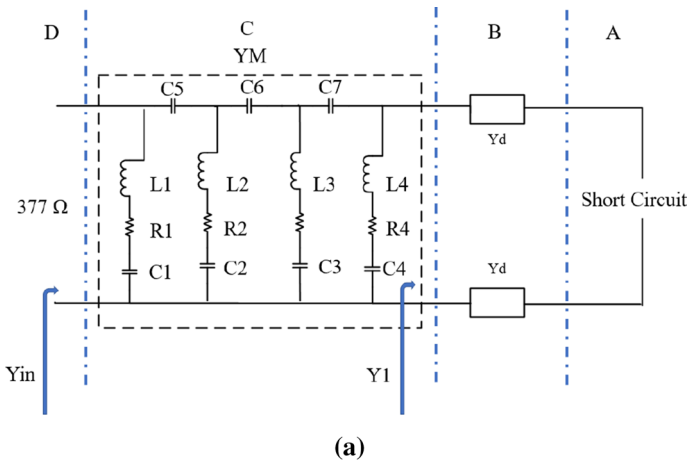


Fig. 4 **a** Circuit equivalent to the proposed structure **b** Circuit schematic of the proposed structure

these resonators. Since the proposed adsorber has four absorption peaks, then part C of the equivalent circuit consists of four series resonators that are parallel to each other. Finally, part D is the free space impedance ($Z_0 \approx 377 \Omega$). It is important to note that if the internal impedance Z_{in} of the equivalent circuit and the impedance of the free space Z_0 are equal, we will have maximum absorption of 100%. Since no structure operates in its ideal state, the proposed absorber also provides the best absorption state for four peaks with a high absorption rate. The transmission line model, interconnected lines are equivalent to a series inductor and resistance, and the distance between the two metals is equal to the capacitor. Figure 4b depicts areas of the proposed absorber structure that represents the capacitor, inductor, and resistance.

The following equations are used to calculate transmission line elements (Asli Nezhad 2020; Nejat and Nozhat 2019):

$$Y_0 = \frac{1}{Z_0} \quad (2)$$

$$Y_{in} = Y_1 + Y_m \quad (3)$$

$$Y_d = \sqrt{\frac{\epsilon_0 \epsilon_r}{\mu_0 \mu_r}} \quad (4)$$

$$Y_1 = Y_d \coth \left[j \frac{\omega}{C_0} d \sqrt{\epsilon_r \mu_r} \right] \quad (5)$$

$$Y_m = G_m + jB_m \quad (6)$$

$$G_m = Y_{in} - \operatorname{Re}(Y_1) = Y_0 - \operatorname{Re}(Y_1) \quad (7)$$

$$B_m = -\operatorname{Im}(Y_1) \quad (8)$$

$$Y_{in} = Y_1 + Y_m \quad (9)$$

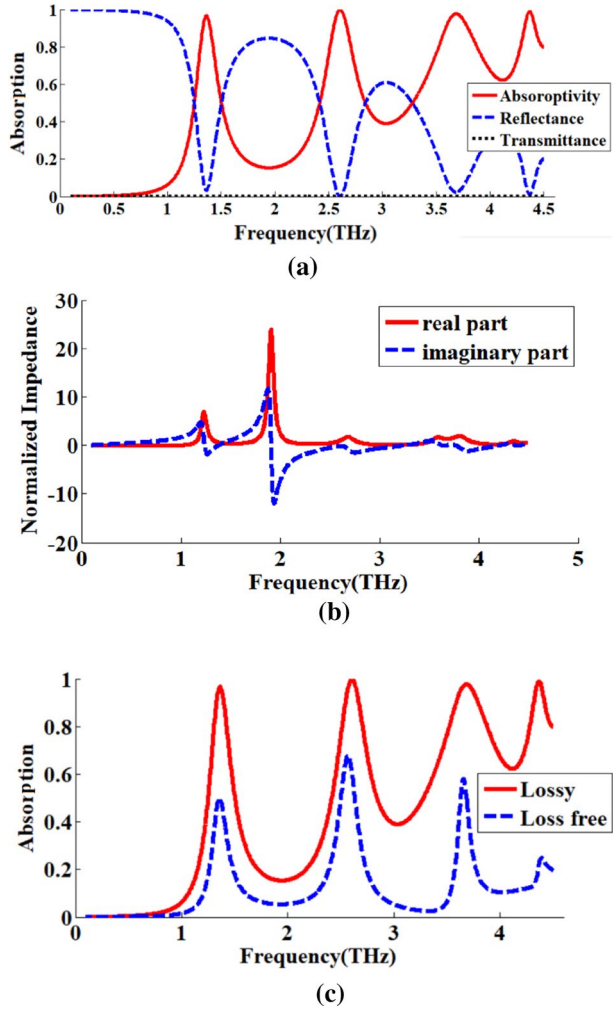
$$A(\omega) = 1 - \Gamma = 1 - \left| \frac{Z_{in} - Z_0}{Z_{in} + Z_0} \right|^2 \quad (10)$$

2.1 Results and discussion

The function of the proposed absorber is such that in the normal occurrence of light has four absorption peaks. As shown in Fig. 5a, the proposed structure has four distinct absorption peaks of 96.46%, 99.82%, 97.74%, and 98.86% in frequencies of 1.36, 2.6, 3.68, and 4.36 THz, respectively. Usually, in multi-band absorbers, the average absorption percentages are expressed. This structure has an average absorption of 98.22%, which can be said with certainty that it is a perfect metamaterial absorber. As shown in Fig. 1, the absorber structure consists of a circle and a square, which are connected by a strip. The first and last resonance frequencies are related to the square shape and the second and third resonance frequencies are related to the presence of the circle in the proposed absorber structure. It is also seen in Fig. 5a, that the reflection decreases the absorption increases at frequency region between the two higher frequency absorption peaks, compared with the region between the two lower frequency absorption peaks. According to equation one, which is given in the article, to reach the maximum absorption peak, the amount of reflection and transmission must be equal to zero. In places where the absorption peak is maximum, the amount of reflection and transmission is at their lowest point. Since the end layer of the structure is made of gold, the transmission value is zero. To minimize the reflection coefficient, the impedance must be matched between the intrinsic impedance of the air and the impedance seen from the input of the proposed absorber structure.

As a result, in places where the absorption rate is low and the reflection is high, it indicates that there is an impedance mismatch at this frequency, at frequencies where the

Fig. 5 **a** The simulated results of proposed absorber **b** the normalized characteristic impedance curve in terms of frequency **c** absorption spectra of the proposed absorber on two different loss conditions



absorption rate is high and the reflection rate is low, it indicates a complete impedance matching between air and the impedance seen from the input of the proposed absorber structure. To justify the above, the normalized characteristic impedance curve in terms of frequency is shown in Fig. 5b. As can be seen at frequencies where the peak absorption is maximum, the real part of the normalized impedance is close to one and the imaginary part is close to zero. For example, the absorption peak at a frequency of 2.6 THz is 99.99%, in which the real part of the impedance is equal to 1.005 and its imaginary part is equal to -0.08, which shows that the impedance is well matched. But at frequencies like 3 terahertz, where the absorption rate is about 40%, the real part of the normalized impedance is 0.16 and the imaginary part is -0.6. These values indicate that the impedance matching is not complete at this frequency, the better the impedance matching, the higher the absorption and the lower the reflection.

Next, we investigate the source of losses in the proposed absorber structure. Figure 5c shows the absorption spectrum of the proposed absorber under two loss conditions (losses

Fig. 6 The absorption spectra for different dielectric heights

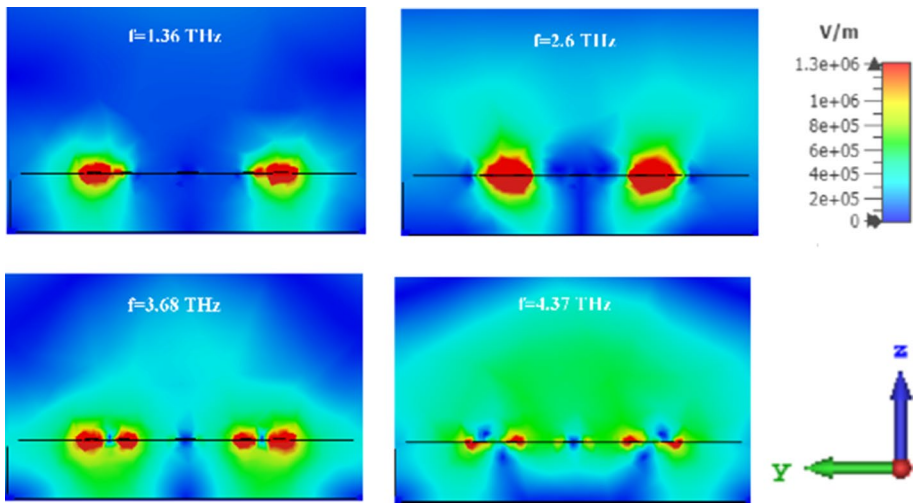
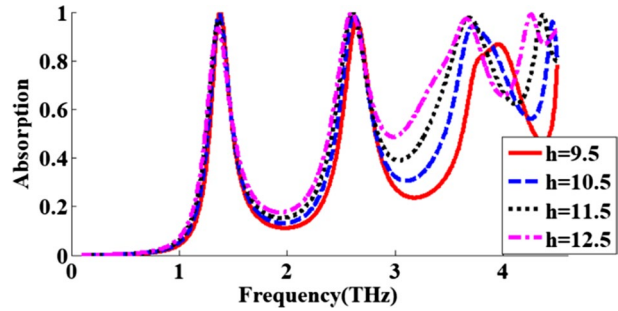


Fig. 7 The electric field distribution at **a** $f = 1.36$ THz, **b** $f = 2.6$ THz, **c** $f = 3.68$ THz, **d** $f = 4.36$ THz

and no losses) of the dielectric layer. From the simulation results, the absorption peaks positions are unchanged with the change of loss conditions, which is by previous reports (Yi et al. 2019; Hu et al. 2016; Chen and Fan 2015).

Also, to investigate the effect of dielectric thickness on the absorption peaks, the dielectric height was also examined, the results of that are illustrated in Fig. 6.

The highest average absorption was obtained for dielectric with a height of 11.5 μm . The primary roots of resonances in this proposed absorber depends on to two factors. 1- electrical dipole 2- electrical quadrupole. The electric field distribution is illustrated in Fig. 7. As can be clearly seen in this figure, the nature of resonance at frequencies 1.36 and 2.36 THz is due to electrical dipole but the nature of resonance at 3.68 and 4.36 THz frequencies is due to the electrical quadrupole.

The distribution of the magnetic field at the four frequencies corresponding to the peaks of the absorption curve of the proposed structure is also illustrated in Fig. 8. As shown in this figure, at 1.36 THz, most of the magnetic field is concentrated at the outer edges of the square. At 2.6 THz, most of the magnetic field is focused on the circle. The physical origin of resonance at both frequencies is an electrical dipole. At 3.68 THz, the focus of the magnetic field is on the side edges of the square.

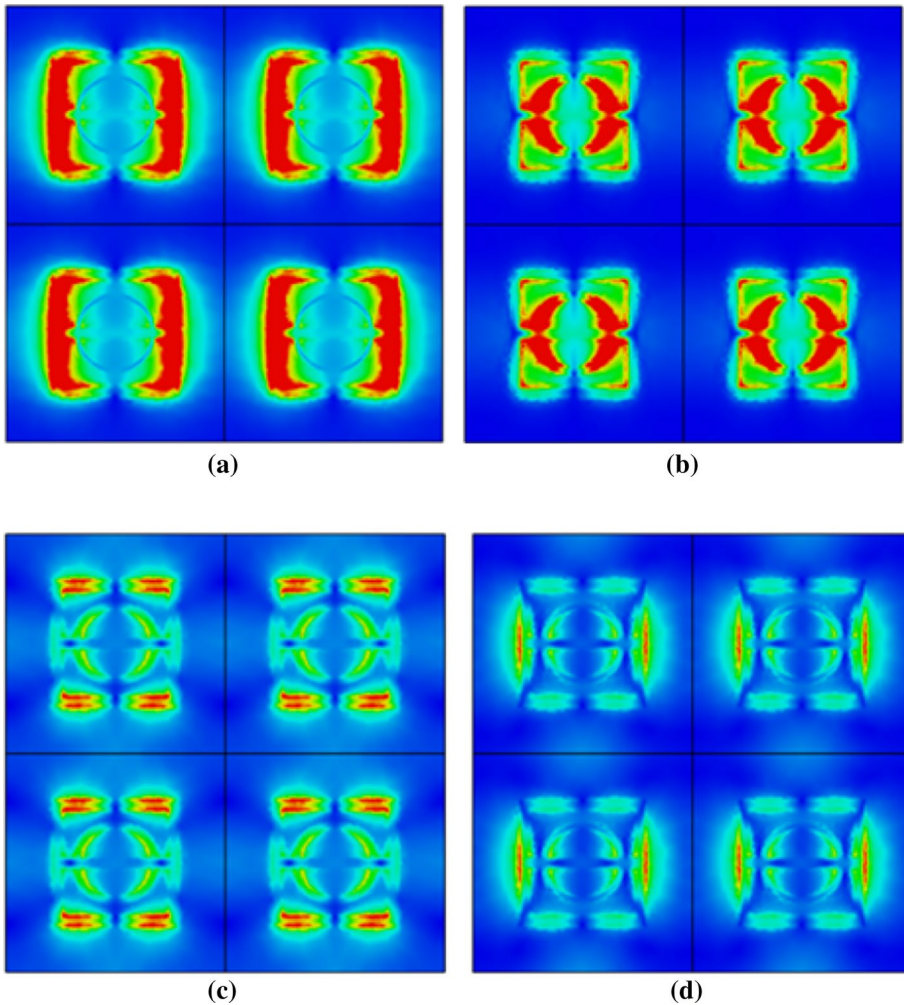
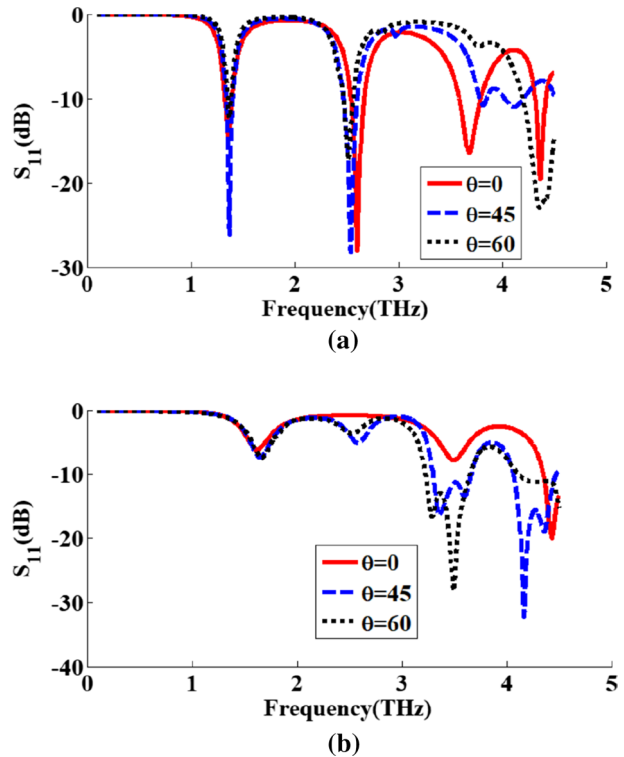


Fig. 8 In the normal incidence the four model structures in z-component magnetic field [real (Hz)] distributions at frequency of **a** $f = 1.36$ THz, **b** $f = 2.6$ THz, **c** $f = 3.68$ THz, **d** $f = 4.36$ THz

As can be seen in Fig. 9, in TE mode, the S_{11} parameter in the range of 2.54 to 2.68 THz is less than -10 dB, which it shows that in this frequency range the absorption rate is perfect, but in the same frequency interval and in TE mode, the value of this parameter is 0 dB, which it indicates that in mode and this frequency interval, no absorption takes place in the structure, while this interval is one of the absorber performance ranges. Also, for different incident angles, S_{11} curve is drawn for this absorber and for two modes, TE and TM, which shows that by changing the incident in TM mode, the absorption rate increases slightly during this period. As a result, the proposed absorber bandgap is in the range of 2.54 to 2.68 THz in TM mode and in normal radiation.

To further investigate the performance of the proposed absorber, we investigate the absorption spectrum as a function of the polarization angle for a TE mode in which the incident angle is fixed at zero degrees and the incident angle of the radiation wave. These

Fig. 9 S₁₁ curve in terms of frequency **a** TE mode **b** TM mode



angles are very influential in the percentage of adsorption of the proposed absorbers. In optical absorbers, the polarization angle is the angle between the X-axis and the polarized direction, which is equivalent to the rotation of the proposed absorber when the polarization direction is constant. Also, the incident angle is the angle between the wave vector and the Z-axis. As shown in Fig. 10, the proposed absorber is sensitive to the polarization angle of the incident terahertz wave.

Therefore, we can use this proposed absorber to adjust the absorption intensity by changing the polarization of the incident wave. These properties make this structure widely used in applications related to wave polarization manipulation and detection of electromagnetic waves with special polarization.

Fig. 10 Dependence of the absorption spectra on the polarization angles of the normally incident wave with TE radiation

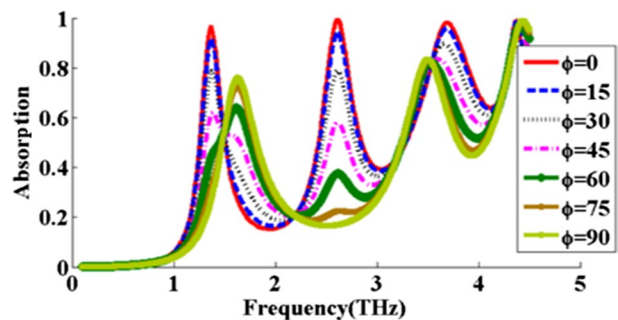


Fig. 11 Dependence of the absorption spectra on the incident angles with TE radiation

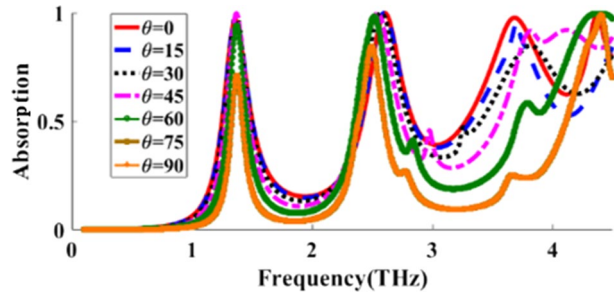
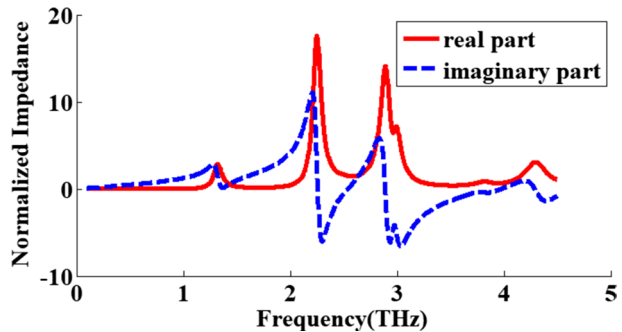


Fig. 12 The normalized characteristic impedance curve in terms of frequency at 45° incident angle



As shown in Fig. 11, the two first absorption peaks are not highly dependent on the incident angle, the two absorption peaks, which are related to higher frequencies, are strongly dependent on the incident angle. For example, as shown in Fig. 11, the amplitude of the third and fourth frequencies is reduced at a 45° incident angle. To investigate the reason, the normalized impedance curve in terms of frequency is shown in Fig. 12.

As can be seen in this figure, at 4 THz the real part of the impedance is 0.7 and the imaginary part of the impedance is 0.08, which indicates that the impedance matching has taken place but is not complete. At 2.6 THz, the real part of the impedance is 1.004 and the imaginary part of the impedance is 0.075, which indicates a perfect impedance matching. Finally, the compared performances of the proposed absorber and the previous works are collected in Table 1.

3 Conclusion

In this paper, a quad-band perfect absorber with an average absorption of 98.22% in four frequencies of 1.36 THz, 2.6 THz, 3.68 THz, and 4.36 THz is introduced. As discussed, this is a classic absorber structure consisting of three layers of metal-dielectric-metal and its dielectric layer is made of SiO₂ material. The SiO₂ dielectric layer is a lossy material, and its difference from the loss-free material was clearly shown. In addition, to better understand the absorption performance of the proposed structure, the electric and magnetic fields of this structure are displayed at all frequencies. Due to its four perfect bands, this absorber has the potential for imaging, sensing, and photodetector applications.

Table 1 The compared performances of the proposed absorber and the previous works

References	Frequency (THz)	Cell size (μm)	Peak numbers	Average absorption (%)
Kiani et al. (2021c)	2.7, 3.2, 3.99, 4.6	3×3	4	99.43
Jafari Chashmi et al. (2019)	0.85, 3.37	15×15	2	95.15
Zamzam et al. (2021)	0.77, 1.13, 1.53, 2.06	85×85	4	97.89
Aghaee and Orougi (2021)	1.59, 2.45, 3.05, 4.41, 5.11	58×58	5	97.35
Mishra and Panwar (2020)	0.53, 0.84, 0.98	200×200	3	92.73
Soheilifar (2018b)	0.72, 1.4, 2.3	42×42	3	90.66
Aloia et al. (2016)	7.75, 14.85, 23.43	2.5×2.5	3	99
Proposed	1.36, 2.6, 3.68, 4.36	70×70	4	98.22

Acknowledgements This research was supported by Semnan University. Also, the authors would like to thank the editor and reviewers for their constructive comments.

Funding No funding was received for this research.

Data availability All data generated or analyzed during this study are included in this published article.

Declarations

Informed consent Written informed consent for participate was obtained from all participants.

Conflict of interest The authors declare that they have no conflict of interest.

Ethical approval We declare that this article is original, has not been published before, and is not currently considered for publication elsewhere. We confirm that the manuscript has been read and approved by all named authors and that there are no other persons who satisfied the criteria for authorship but are not listed. We further confirm that the order of authors listed in the manuscript has been approved by all of us.

References

- Aghaee, T., Orougi, A.A.: dual-band terahertz absorber based on graphene periodic arrays of disks and ribbons: circuit model approach. *J. Comput. Electron.* **20**, 611–625 (2021)
- Alizadeh, S., Zareian-Jahromi, E., Mashayekhi, V.: A tunable graphene-based refractive index sensor for THz bio-sensing applications. *Opt. Quant. Electron.* **54**(2), 1–13 (2022)
- Aloia, D., et al.: Adaptive broadband radar absorber based on tunable graphene. *IEEE Trans. Antennas Propag.* **64**, 2527–2531 (2016)
- Arezoomand, A.S., et al.: Independent polarization and multi-band THz absorber base on Jerusalem cross. *Opt. Commun.* **352**, 121–126 (2015)
- Askari, M.: A near infrared plasmonic perfect absorber as a sensor for hemoglobin concentration detection. *Opt Quant. Electron.* **53**, 67 (2021)
- Askari, M., Hosseini, M.V.: Infrared metamaterial refractive-index-based sensor. *JOSA B* **37**(9), 2712–2718 (2020a)
- Askari, M., Hosseini, M.V.: A novel metamaterial design for achieving a large group index via classical electromagnetically induced reflectance. *Opt. Quant. Electron.* **52**, 191 (2020b)

- Asli Nezhad, M.: High sensitivity refractive index and temperature sensor based on semiconductor metamaterial perfect absorber in the terahertz band. *Opt. Commun.* **463**, 125411 (2020)
- Bian, L.A., et al.: Controllable multi-mode absorption in terahertz absorber with graphene-dielectric-stack strips. *Superlattice Microst.* **150**, 106784 (2021)
- Chen, Z., Fan, W.: Ultra-flexible polarization-insensitive multiband terahertz metamaterial absorber. *Appl. Opt.* **54**, 2376–2382 (2015)
- Danaeifar, M., Granpayeh, N.: Graphene-based polarization-sensitive metasurfaces for integrated optics applications. *Appl. Opt.* **59**, 10541–10546 (2020)
- Ebrahimi, S.: Optical absorber based on self-similar cylindrical element for detecting optical material. *Opt. Quant. Electron.* **52**, 87 (2020)
- Esfandiari, M., et al.: Enhancing the sensitivity of a transmissive graphene-based plasmonic biosensor. *Appl. Opt.* **60**, 1201–1208 (2021)
- Ghods, M.M., Rezaei, P.: Graphene-based Fabry-Perot resonator for chemical sensing applications at mid-infrared frequencies. *IEEE Photon. Technol. Lett.* **30**, 1917–1920 (2018a)
- Ghods, M.M., Rezaei, P.: Ultra-wideband microwave absorber based on uncharged graphene layers. *J. Electromag. Wav. Appl.* **32**, 1950–1960 (2018b)
- Ghosh, S., Kumar, V.S.: A polarization-independent broadband multilayer switchable absorber using active frequency selective surface. *IEEE Antennas Wirel. Propag. Lett.* **16**, 3147–3150 (2017)
- Hu, D., et al.: Design of four-band terahertz perfect absorber based on a simple #-shaped metamaterial resonator. *Appl. Phys. a.* **122**, 1–7 (2016)
- Ikram, M., Nghia, N., Abbosh, A.: Hybrid antenna using open-ended slot for integrated 4G/5G mobile application. *IEEE Antennas Wirel. Propag. Lett.* **19**, 710–714 (2020)
- Jafari Chashmi, M., Rezaei, P., Kiani, N.: Polarization controlling of multi resonant graphene-based microstrip antenna. *Plasmonics*, 15 (2020a) 417–426.
- JafariChashmi, M., Rezaei, P., Kiani, N.: Reconfigurable graphene-based V-shaped dipole antenna: From quasi-isotropic to directional radiation pattern. *Optik* **184**, 421–427 (2019)
- JafariChashmi, M., Rezaei, P., Kiani, N.: Y-shaped graphene-based antenna with switchable circular polarization. *Optik* **200**, 163321 (2020b)
- W. Jiang and T. Chen, A five-band absorber based on graphene metamaterial for terahertz ultra-sensing. *Nanotechnol* (2022) 33:165503.
- Kazemi, F.: High Q-factor compact and reconfigurable THz aperture antenna based on graphene loads for detecting breast cancer cells. *Superlattice. Microst.* **153**, 106865 (2021)
- Khani, S., et al.: Tunable compact microstrip dual-band bandpass filter with tapered resonators. *Microw. Opt. Technol. Lett.* **60**, 1256–1261 (2018)
- Khani, S., Danaie, M., Rezaei, P.: Tunable single-mode bandpass filter based on metal–insulator–metal plasmonic coupled U-shaped cavities. *IET Optoelectron.* **13**, 161–171 (2019)
- Khani, S., Danaie, M., Rezaei, P.: Realization of a plasmonic optical switch using improved nano-disk resonators with Kerr-type nonlinearity: A theoretical and numerical study on challenges and solutions. *Opt. Commun.* **477**, 126359 (2020a)
- Khani, S., Danaie, M., Rezaei, P.: Compact and low-power all-optical surface plasmon switches with isolated pump and data waveguides and a rectangular cavity containing nano-silver strips. *Superlattice. Microst.* **141**, 106481 (2020b)
- Khani, S., Danaie, M., Rezaei, P.: Plasmonic all-optical metal–insulator–metal switches based on silver nano-rods. *J. Comput. Electron.* **20**, 442–457 (2021)
- Khatami, S.A., et al.: Compact via-coupling fed monopulse antenna with orthogonal tracking capability in radiation pattern. *IEEE Antennas Wirel. Propag. Lett.* **19**, 1443–1446 (2020)
- Kiani, S., Rezaei, P., Navaei, M.: Dual-sensing and dual-frequency microwave SRR sensor for liquid samples permittivity detection. *Measurement* **160**, 107805 (2020)
- Kiani, S., Rezaei, P., Fakhr, M.: A CPW-fed wearable antenna at ISM band for biomedical and WBAN applications. *Wirel. Networks* **27**, 735–745 (2021a)
- Kiani, S., Rezaei, P., Navaei, M.: An overview of interdigitated microwave resonance sensors for liquid samples permittivity detection, Springer. *Nature* **7**, 153–197 (2021b)
- Kiani, N., Hamedani, F.T., Rezaei, P.: Polarization controlling method in reconfigurable graphene-based patch four-leaf clover-shaped antenna. *Optik* **231**, 166454 (2021c)
- Kundu, D., Mohan, A., Chakrabarty, A.: Single-layer wideband microwave absorber using array of crossed dipoles. *IEEE Antennas Wirel. Propag. Lett.* **15**, 1589–1592 (2016)
- Landy, N., et al.: Perfect metamaterial absorber. *Phys. Rev. Lett.* **100**(20), 207402 (2008)
- Lim, D., Sungjoon, L.: Ultrawideband electromagnetic absorber using sandwiched broadband metasurfaces. *IEEE Antennas Wirel. Propag. Lett.* **18**, 1887–1891 (2019)

- Meng, H., et al.: Tunable graphene-based plasmonic multispectral and narrowband perfect metamaterial absorbers at the mid-infrared region. *Appl. Opt.* **56**, 6022–6027 (2017)
- Meng, H.Y., et al.: A simple design of a multi-band terahertz metamaterial absorber based on periodic square metallic layer with T-shaped gap. *Plasmonics* **13**, 269–274 (2018)
- Mishra, R., Panwar, R.: Investigation of graphene fractal frequency selective surface loaded terahertz absorber. *Opt. Quant. Electron.* **52**, 317 (2020)
- Mousavi, Z., Rezaei, P., Rafii, V.: Single layer CPSSA array with change polarization diversity in broadband application. *Int. J. RF Microw. Comput. Aided Eng.* **27**(4), e21075 (2017)
- Mousavi, Z., et al.: Beam-steering antenna array based on a butler matrix feed network with CP capability for satellite application. *J. Instrument.* **14**, P07005 (2019)
- Nejat, M., Nozhat, N.: Ultrasensitive THz refractive index sensor based on a controllable perfect MTM absorber. *IEEE Sens. J.* **19**, 10490–10497 (2019)
- Norouzi-Razani, A., Rezaei, P.: Broadband polarization insensitive and tunable terahertz metamaterial perfect absorber based on the graphene disk and square ribbon. *Micro Nanostruct.* **163**, 107153 (2022)
- Sharbati, V., Rezaei, P., Fakharian, M.M.: A planar UWB antenna with switchable single/double band-rejection characteristics. *Radioeng. J.* **25**, 429–435 (2016)
- Shimatani, M., et al.: Turbostratic stacked graphene-based high-responsivity mid-wavelength infrared detector using an enhanced photogating effect. *Opt. Mater. Express* **12**(2), 458–467 (2022)
- Soheilifar, M.R.: Wideband optical absorber based on plasmonic metamaterial cross structure. *Opt. Quant. Electron.* **50**, 442 (2018a).
- Soheilifar, M.R.: Wideband optical absorber based on plasmonic metamaterial cross structure. *Opt. Quant. Electron.* **50**, 442 (2018b)
- Upender, P., Kumar, A.: Design of a multiband graphene-based absorber for terahertz applications using different geometric shapes. *JOSA B* **39**(1), 188–199 (2022)
- Wang, G.Z., Wang, B.: Five-band terahertz metamaterial absorber based on a four-gap comb resonator. *J. Lightwav. Technol.* **33**, 5151–5156 (2015)
- Yi, Z., et al.: Graphene-based tunable triple-band plasmonic perfect metamaterial absorber with good angle-polarization-tolerance. *Res. Phys.* **13**, 102149 (2019)
- Yu, J.W., Cai, Y., Lin, X.Q., Wang, X.: Perforated multilayer ultra wideband absorber based on circuit analog absorber with optimal air spaces. *IEEE Antennas Wirel. Propag. Lett.* **19**, 34–38 (2019)
- Zamzam, P., Rezaei, P.: A terahertz dual-band metamaterial perfect absorber based on metal-dielectric-metal multi-layer columns. *Opt. Quant. Electron.* **53**, 109 (2021)
- Zamzam, P., Rezaei, P., Khatami, S.A.: Quad-band polarization-insensitive metamaterial perfect absorber based on bilayer graphene metasurface. *Phys. E Low Dimens. Syst. Nanostruct.* **128**, 114621 (2021)
- Zhou, P., et al.: A stretchable metamaterial absorber with deformation compensation design at microwave frequencies. *IEEE Trans. Antennas Propag.* **67**, 291–297 (2018)

Publisher's Note Springer Nature remains neutral with regard to jurisdictional claims in published maps and institutional affiliations.

Springer Nature or its licensor holds exclusive rights to this article under a publishing agreement with the author(s) or other rightsholder(s); author self-archiving of the accepted manuscript version of this article is solely governed by the terms of such publishing agreement and applicable law.